Since January 2020 Elsevier has created a COVID-19 resource centre with free information in English and Mandarin on the novel coronavirus COVID-19. The COVID-19 resource centre is hosted on Elsevier Connect, the company's public news and information website.

Carbohydrate Polymer Technologies and Applications 3 (2022) 100182

Contents lists available at ScienceDirect

Carbohydrate Polymer Technologies and Applications

journal homepage: www.sciencedirect.com/journal/carbohydrate-polymer-technologies-and-applications

Hydrophobic cellulose-based and non-woven fabrics coated with mesoporous TiO_2 and their virucidal properties under indoor light

Darliane CS Souza [a], Suélen M Amorim [b], Rafael D Cadamuro [c], Gislaine Fongaro [c], Rosely A Peralta [b], Rosane M Peralta [d], Gianluca Li Puma [e], Regina FPM Moreira [a,*]

[a] Laboratory of Energy and Environmental Processes, Department of Chemical Engineering and Food Engineering, Federal University of Santa Catarina, 88040-900, Florianópolis, SC, Brazil
[b] Laboratory of Bioinorganic and Crystallography, Department of Chemistry, Federal University of Santa Catarina, 88040-900, Florianópolis, SC, Brazil
[c] Laboratory of Applied Virology, Department of Microbiology, Immunology and Parasitology, Federal University of Santa Catarina, 88040-900, Florianópolis, SC, Brazil
[d] Department of Biochemistry – State University of Maringá, Maringá – PR, Brazil
[e] Environmental Nanocatalysis & Photoreaction Engineering, Department of Chemical Engineering, Loughborough University, Loughborough, United Kingdom

ARTICLE INFO

Keywords:
Titanium dioxide hydrosol
Human coronavirus and adenovirus
Virucidal effect
Textiles
Nanoparticles
Sol-gel synthesis

ABSTRACT

Antiviral hydrophobic cellulose-based cotton or non-woven fabrics containing mesoporous TiO_2 particles were developed for potential use in healthcare and in other contaminated environments. Hydrosols made with the sol-gel method using two different amounts of the Ti precursor were applied to cotton and non-woven fabrics and their virucidal effect on Murine Coronavirus (MHV-3) and Human Adenovirus (HAdV-5) was evaluated under indoor light irradiation. The results show 90% reduction of HAdV-5 and up to 99% of MHV-3 in non-woven fabric, and 90% reduction of MHV-3 and no reduction of HAdV-5 in cotton fabric. The antiviral activity was related to the properties of the TiO_2 powders and coatings characterized by BET surface area, DRX, DLS, FTIR, DRS, SEM, TEM and water contact angle. The hydrophobic characteristic of the treated fabrics and the high surface area of the TiO_2 particles favor interaction with the virus, especially MHV-3. These results demonstrate that non-woven fabric and cotton, coated with TiO_2, can be highly effective in preventing contamination with MHV-3 and HAdV-5 viruses, particularly for applications in healthcare indoor environments.

1. Introduction

Nanoparticles are among the studied materials in the area of antimicrobial applications, having demonstrated a great potential for the disinfection/inactivation of harmful pathogens, including bacteria, viruses, and fungi (Hamouda et al., 2021; Hosseini, Chin, Behzadinasab, Poon & Ducker, 2021; Park et al., 2014; Rodríguez-González, Obregón, Patrón-Soberano, Terashima & Fujishima, 2020; Uyguner Demirel, Birben & Bekbolet, 2018; Zan, Fa, Peng & Gong, 2007). Among different nanoparticles, TiO_2 has demonstrated biocidal effect for numerous microorganisms (Hosseini et al., 2021; Park et al., 2014; Rodríguez-González et al., 2020; Uyguner Demirel et al., 2018; Zan et al., 2007) including gram-positive and gram-negative bacteria (Dicastillo, de, Correa, Martínez, Streitt & Galotto, 2020; Ibrahim et al., 2018; Ibrahim, Eid, El-Aziz, Abou Elmaaty & Ramadan, 2017; N. A. Ibrahim, Eid, Khalil & Almetwally, 2018), various viral species and parasites (Rodríguez-González et al., 2020).

The antiviral behavior of TiO_2 nanoparticles is, however, less documented than its antibacterial properties. In particular, the antiviral activity of TiO_2 has been investigated against the influenza virus (H3N2) and against bacteriophages such as MS2, PRD1 or ϕX174 (Gerrity, Ryu, Crittenden & Abbaszadegan, 2008; Mazurkova et al., 2010; Syngouna & Chrysikopoulos, 2017). Increasing concerns about the spread of epidemic and pandemic viral diseases have drawn the attention towards the development of photocatalytic nanotechnologies particularly for application in hospital settings. Recently, Khaiboullina, Uppal, Dhabarde, Subramanian and Verma (2020) reported that surfaces coated with titanium dioxide, a thin, nontoxic layer applied as paint, can enhance surface disinfection of human coronaviruses, under UV light. Similarly, Moon, Lee, Rok and Ha (2020) demonstrated that viral particles of HuNoVs could efficiently be disinfected using Cu/TiO_2-treated non-woven fabric under UVA-LED.

Mechanistically, it has been reported that photocatalytic viral disinfection occurs through three possible steps: (1) particle shape

* Corresponding author: https://orcid.org/0000-0002-2863-7260.
E-mail address: regina.moreira@ufsc.br (R.F. Moreira).

https://doi.org/10.1016/j.carpta.2021.100182
Received 18 August 2021; Received in revised form 24 December 2021; Accepted 28 December 2021
Available online 30 December 2021

distortion, (2) protein oxidation, and (3) gene leakage or damage. In the first step, the adsorption of a virus on the photocatalytic surface could distort the virus' shape (Li et al., 2016; Moon et al., 2020) causing the rupture of the viral capsid proteins, and possibly leading to gene efflux. In parallel, the oxidation of proteins by reactive oxygen species (ROS) (such as $^{\bullet}OH$, $^{\bullet}O_2$ and $HO^{\bullet}_2$) produced by a TiO_2 photocatalyst under light irradiation (N. A. Ibrahim, Aly, Eid & Fahmy, 2018; Khezerlou, Alizadeh-Sani, Azizi-Lalabadi & Ehsani, 2018; Y. Liu, Huang, Feng & Li, 2021; Rodríguez-González et al., 2020) can also destroy the virus outer envelope and the capsid protein of the viruses, resulting in the release of its genetic materials (Kumar & Devi, 2011; Li et al., 2016; Moon et al., 2020; Syngouna & Chrysikopoulos, 2017). Finally, viral inactivation can also result from induced toxicity by metal ions in metal-containing photocatalysts, such as Ag/TiO_2, Cu-TiO_2, Pt-WO_3, C_{60}-magnetite, Mn-TiO_2, Co-TiO_2, among others (Hosseini et al., 2021; Kumar & Devi, 2011; Mohan, Hemalatha, Kopperi, Ranjith & Kumar, 2021). The general consensus is that virus inactivation depends on the characteristics of each microorganism (sizes, shapes, structures or compositions), exposure time and on the characteristics of the TiO_2 particles, among other aspects (Khezerlou et al., 2018; Y. Liu et al., 2021; Rodríguez-González et al., 2020). Light irradiation is generally essential in photocatalysis to increase the rate of virus inactivation (Rodríguez-González et al., 2020). However, the germicidal effect has also been observed under darkness (Erdem, Metzler, Cha & Huang, 2015; Syngouna & Chrysikopoulos, 2017). Despite the suggested mechanisms has been related to the wetting property of nanoparticles (Liu, John, Yeung & Si, 2007) and/or the adsorptive properties of these (De Pasquale et al., 2020; Liu et al., 2021) the underlying mechanism has not been thoroughly elucidated (Syngouna & Chrysikopoulos, 2017).

The material used to support TiO_2 can significantly contribute to promoting the interaction between viruses and particles. Cellulose-based fabrics such as cotton and non-woven fabrics have been widely studied for the application of titanium dioxide hydrosols, resulting in fabrics with photocatalytic and self-cleaning properties (Ahmad, Kan & Yao, 2019; Ibrahim et al., 2017; N. A. Ibrahim et al., 2018, 2018, 2018; Moon et al., 2020; Rashid, Simoncic & Tomsic, 2021; Tan, Gao, Guo, Guo & Long, 2013; Wang, Dong, Li, Li & Bian, 2018). Properties such as porosity, flexibility and layered surface structure contribute to the incorporation of nanoparticles in its structure, providing new functional properties (Ahmad et al., 2019).

In this study, two different virus strains were used to evaluate the inactivation effect caused by fabrics coated with TiO_2: the human adenovirus type 5 (HAdV-5) which has an icosahedral capsid formed by proteins (Alonso-Padilla et al., 2016), and the murine coronavirus three viral proteins, and the genome packaged in a helical nucleocapsid surrounded by a host-derived lipid bilayer (Belouzard, Millet, Licitra & Whittaker, 2012). These viruses are representative targets to ensure virucidal activity of materials (International Organization for Standardization, 2019). Non-enveloped viruses (such as adenoviruses, noroviruses, human enteroviruses, among others) are generally more resistant to disinfectants and antiseptics and ultraviolet radiation than enveloped viruses (Metcalf, Melnick & Estes, 1995; Rabenau, Steinmann, Rapp, Schwebke & Eggers, 2014). Moreover, human adenovirus is currently being explored as vaccine vectors for coronavirus disease (COVID-19) (Person et al., 2021), and murine coronavirus represents a suitable model for study coronavirus virulence factors, multiorgan involvement and antiviral immunity (Grabherr, Ludewig & Pikor, 2021).

The photocatalytic virucidal effect of high surface area mesoporous TiO_2 immobilized on textile fabrics (cellulose-based cotton and polypropylene non-woven fabrics, commonly used in hospital settings) was investigated. The inactivation of Murine Coronavirus (MHV-3) and Human Adenovirus (HAdV-5) was determined under typical indoor irradiation encountered in healthcare indoor environments and according to the ISO 18,184:2019 standard test method for virucidal activity. The virucidal effects of the coatings were correlated to the physical and chemical properties of the TiO_2 coatings to gain a deeper understanding of the impact of catalyst properties on the inactivation of MHV-3 and HAdV-5 in coated fabrics.

2. Experimental

2.1. Materials

Cellulose-based cotton (166 ± 5 g m^{-2}) and polypropylene non-woven (40 ± 4 g m^{-2}) fabrics were purchase from a local market in Santa Catarina (Brazil). Titanium butoxide was provided by Sigma – Aldrich (97%). The acetic acid (99.5%) and ethanol (99.8%) were obtained from Lafan (Brazil) and Neon (Brazil), respectively. The fabrics and reagents were used without prior treatment/purification.

2.2. Synthesis of TiO_2 hydrosol and textile treatments

The titanium dioxide hydrosol synthesis were conducted as proposed by Wang et al. (2018). Initially, 5.54 mL of titanium butoxide [$Ti(OBu)_4$] and 2.46 mL of ethanol were added to a beaker and stirred for 1 h (solution 1). Subsequently, 5.72 mL of acetic acid and 36.14 mL of deionized water (solution 2) were added to another beaker and the pH was measured (pH ~ 1.96). Solution 1 was added dropwise to solution 2 and agitated for 3 h. The resulting hydrosol solution (TiO_2 hydrosol-S1, solids concentration 33.02 mg L^{-1}) was stored at room temperature for 10 days. Further, another TiO_2 hydrosol sample (TiO_2 hydrosol-S2, solids concentration 17.28 mg L^{-1}) was prepared using the same procedure but half the amount of [$Ti(OBu)_4$], i.e. 2.77 mL. Translucent yellowish-white colloidal hydrosols were obtained. After the preparation of the hydrosols, pristine cotton and polypropylene non-woven fabrics (2 × 2 cm) were then submerged for 5 min into the TiO_2 hydrosols, and subsequently, the impregnated fabrics were cured in an oven at a temperature of 100 °C for approximately 12 h. The amount of TiO_2 per square centimeter loaded on each fabric sample was calculated by mass balance. Untreated fabric samples (without TiO_2 deposition) were also subjected to the same protocol and further used in the photocatalytic tests, as controls. The fabric samples were designated as shown in Table 1.

The physical and chemical properties of the TiO_2 coated onto the fabric were obtained after drying TiO_2 hydrosols in an oven at a temperature of 105 °C for 24 h to obtain white colored TiO_2 powders denoted TiO_2-S1 and TiO_2-S2.

2.3. Testing and characterization of TiO_2 particles and TiO_2 coated fabrics

The crystalline structure of the sample was evaluated by X-Ray diffraction (XRD) analysis using a MiniFlex600 DRX apparatus (Rigaku, Japan), at a scanning speed of 10 ° min^{-1} with step size of 0.05 °. The crystallite sizes, based on the average of all the peaks of the XRD standards, were calculated using the Scherrer' equation:

$$D = \frac{K\lambda}{\beta cos\theta} \quad (1)$$

where D is the size of the crystallites, K is the Scherrer constant (0.9), λ is

Table 1
Treated and untreated fabric samples used to measure virucidal activity.

Fabric	Impregnation	TiO_2 loading, mg cm^{-2}
Untreated cotton (white)	none	0.0
Non-woven fabric (NWF)	none	0.0
TiO_2-S1-cotton	TiO_2 hydrosol-S1	1.40
TiO_2-S1-NWF	TiO_2 hydrosol-S1	1.07
TiO_2-S2-cotton	TiO_2 hydrosol-S2	1.03
TiO_2-S2-NWF	TiO_2 hydrosol-S2	1.04

the wavelength of the radiation used (0.15406 nm), β is the full width at half maximum (FWHM) of selected peak and θ is the Bragg's angle of diffraction for the peak.

The optical properties of the samples were evaluated using the data from the diffuse reflectance spectroscopy (DRS) obtained in a UV/Vis/NIR Lambda 750 spectrometer (PerkinElmer, USA), equipped with a 60 mm integrating sphere. The reflection (R) data were converted to absorption through the Kubelka–Munk function, $F(R)$ (Tan et al., 2013).

$$F(R) = \frac{(1-R)^2}{2R} \quad (2)$$

Infrared spectra were obtained using a Fourier transform infrared (FTIR) spectrophotometer (model Cary 660 Series, Agilent, USA). The samples were analyzed directly with the crystal (ZnSe, 45°) by attenuated total reflection (ATR), averaging 10 scans in the range of 4000–550 cm^{-1} at a resolution of 4 cm^{-1}. The Brunauer–Emmett–Teller (BET) surface area, Barrett–Joyner–Halenda (BJH) pore volume and pore size distributions of the samples were determined via N_2 adsorption–desorption isotherm measurement at 77 K after degassing at 300 °C for 2 h. The isotherms were obtained in a Autosorb-1 gas sorption analyzer (Quantachrome Instrument, USA). The particle size distribution was obtained by the dynamic light scattering (DLS) technique using a Zetasizer Nanosizer particle size analyser (Malvern Instruments, UK). Before analysis, TiO_2 samples (TiO_2-S1 and TiO_2-S2) were dispersed in distilled water (0.1 mg mL^{-1}) using an ultrasound bath for 1 h. The morphology and microstructures of TiO_2 powdered were characterized by Scanning Electron Microscopy-FEG using a FEG-SCIOS (FEI, USA) and by Transmission Electronic Microscopy using a JEM-1011 (JEOL, Japan) equipment.

The surfaces of treated and untreated fabrics were analyzed by scanning electron microscopy (SEM) using a JEOL JSM-6390LV microscope (JEOL, Japan). The contact angle between liquid and solid surfaces of the treated fabrics was conducted with a Goniometer model 250 (Ramé-Hart Instrument, USA). Measurements were performed in triplicate and the angles were determined by the mean of the values obtained. In these analyses, drops of 3 μL of deionized water at room temperature were deposited over each fabric sample.

2.4. Virucidal activity

Coated and uncoated fabrics were previously evaluated for their cytotoxic characteristics. For this, mouse fibroblast cells (L929, ATCC® CCL-1) were maintained in a minimal essential medium (MEM; Thermo Fisher Scientific, Poland) supplemented with 10% heat-inactivated fetal bovine serum (FBS; Thermo Fisher Scientific, Poland), then sown on plates (96-well format plates, 2.5×10^4 cells/well) maintained for 24 h at 37 °C in an atmosphere containing 5% CO_2. Tissues were washed with 5 mL of 1% phosphate-buffered saline and the eluate was added to the cell culture for 48 h.

The virucidal activity of the materials and fabrics were assessed according to the ISO 18,184:2019 and standard method for determination of antiviral activity of textile products (International Organization for Standardization, 2019). Information about the light indoor irradiation is supplied in the Supplementary Information (Figure S1). This method measures the concentration of 10^5 plaque-forming units (PFU) of human adenovirus type 5 (HAdV-5) and murine coronavirus MHV-3 strain (MHV-3), previously propagated in cell lines A549 (human lung carcinoma - CL185) and L929 (murine fibroblasts - CCL-1), respectively.

Tests were performed with 30 min viral exposure against the tested surfaces at 25 °C under indoor light irradiation. Similar control experiments were performed in the absence of light irradiation by exposing the samples to the viruses inside a dark chamber. Both impregnated and pristine fabrics were used. After 5–7 days of *in vitro* infection with the respective viruses tested, the amount of PFU was quantified and the viral reduction was expressed in percent reduction (%) (International Organization for Standardization, 2019). Triplicate experiments were performed for all trials.

To assess the absence of viral replication, in addition to the cell culture test, assays based on detection of the viral genome after 5–7 days of infection in cell culture were performed. This test was carried out to verify whether or not there was entry and exposure of the viral genome in permissive cells, as well as whether these genomes were replicated. In summary, after 5–7 days of incubation the cells with HAdV-5 and MHV-3 fluids after exposure to tissues with and without TiO_2, were washed 3 times with PBS 1X and subjected to extraction of genetic material (DNA / RNA). The extraction of viral nucleic acid was performed with the commercial mini kit RTP DNA / RNA Virus® II (Invitek), according to the manufacturer's instructions. A reverse transcriptase (RT) reaction was performed to generate cDNA from mRNA, using an RT enzyme and primers (Sensiscript RT Kit - QIAGEN®). Real-time quantitative PCR (qPCR) was performed as described by Hernroth, Conden-Hanson, Rehnstan-Holm, Girones and Allard (2002) and Besselsen, Wagner and Loganbill (2003), for HAdV-2 and MHV-3, respectively. The limit of quantification is ten copy gene (CG) per cm^3.

All amplifications were performed in a StepOne Plus® Real-Time PCR system (AppliedBiosystems). Each sample was analyzed in triplicate. Ultrapure water was used as a non-template control for each assay.

3. Results and discussion

3.1. Characterization of pristine TiO_2 particles and of the impregnated and pristine fabrics

The crystalline structure of the TiO_2 powders obtained from hydrosols (TiO_2-S1 and TiO_2-S2) was evaluated by X-ray diffraction (Fig. 1). The crystal phase of all samples coincides with the standard data for anatase -TiO_2 (TiO_2 - JCPDS 01–078–2486) without impurities (Kleebusch et al., 2018). The values of crystallite sizes of TiO_2-S1 and TiO_2-S2 were similar and below the 10-nanometer range (Table 2).

The particle size distribution of TiO_2-S1 was non uniform and ranged from 50 to 1700 nm with a maximum peak at 142 nm, a second peak with a maximum at 532 nm (Fig. 2(a)) and average particle size of 284 nm (Table 2). In contrast, TiO_2-S2 had a uniform particle size distribution (Fig. 2(b)) but in the range of 300 – 1000 nm and a maximum peak at 255 nm, with the average particle size of 263 nm (Table 2). The samples have size distributions in the characteristic range of micrometric particles, that is, 100 nm – 100 μm, indicating that TiO_2 nanoparticles formed aggregates in the aqueous dispersion.

The scanning electron microscopy (SEM-FEG) of powdered TiO_2-S1 and TiO_2-S2 analysis showed the preparation of spherical-shape TiO_2 nanoparticles (Figure S2). The transmission scanning microscopy (TEM) images exhibited aggregated nanoparticles while the selected area diffraction (SAED) patterns endorsed the polycrystalline nature (Figure S2). Particle dimensions obtained from TEM images were 9.7 ±

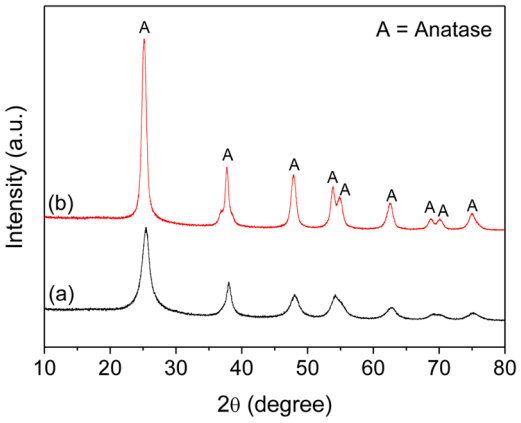

Fig. 1. Diffractograms of (a) TiO_2-S1 and (b) TiO_2-S2 samples.

Table 2
Specific surface area (S_{BET}), average pore diameter, pore volume and average particle size for TiO_2 samples.

Sample	Crystallite size (nm)	Band gap energy (eV)	S_{BET} ($m^2\ g^{-1}$)	Average pore size (Å)	Pore volume ($cm^3\ g^{-1}$)	Average aggregated particle size (nm)**
TiO_2-S1	7.0 ± 1.3	3.16	293.1	43.87	0.3292	284
TiO_2-S2	9.0 ± 1.0	3.17	342.4	37.29	0.3221	263
Uncoated cotton	*	*	<< 1	*	0.010	*
Uncoated NWF	*	*	0.9	938	0.021	*
TiO_2-S1 cotton	*	*	10	60	0.020	*
TiO_2-S1 NWF	*	*	51	44	0.057	*
TiO_2-S2-cotton	*	*	9	29	0.006	*
TiO_2-S2 -NWF	*	*	110	40	0.111	*

* Not measured.
** Obtained by the dynamic light scattering (DLS) technique in aqueous dispersion.

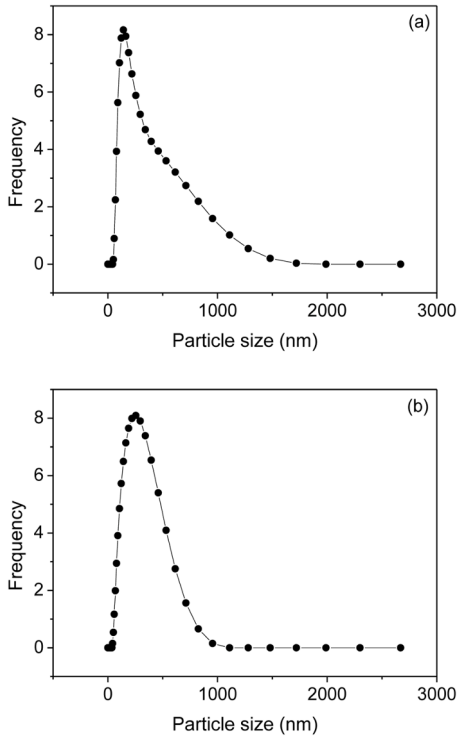

Fig. 2. Particle size distribution of (a) TiO_2-S1 and (b) TiO_2-S2 dispersed in distilled water. $[TiO_2] = 0.1\ mg\ mL^{-1}$.

5.0 nm and 6.5 ± 2.1 nm for TiO_2-S1 and TiO_2-S2, respectively. As largely known, the particle size increases with increasing precursor concentration due to enhanced coagulation and sintering, resulting from the large concentration of TiO_2 nuclei generated at high Ti precursor concentrations (Nyamukamba, Okoh, Mungondori, Taziwa & Zinya, 2018). Moreover, a more uniform particle size distribution was observed for powdered TiO_2-S2 than TiO_2-S1. The particles size calculated from TEM micrographs were slightly different from the average crystallite size obtained from XRD pattern (Table 2), although these were within the experimental deviation.

The optical properties of the uncoated and coated fabrics (cotton and NWF) and TiO_2 powders were evaluated by diffuse reflectance spectroscopy (Fig. 3 and Figure S3). The uncoated fabrics (cotton and NWF) did not show a significant photoresponse, Fig. 3. Conversely, in coated fabrics, reported remarkable absorption in the UV range ($\lambda < 400$ nm). The TiO_2-S1-cotton and TiO_2-S2-cotton curves were integrated in the range below 400 nm, and the areas were 693 and 757, respectively. For the TiO_2-S1-NWF and TiO_2-S2-NWF curves, the areas were 284 and 329, respectively. According to the areas and intensities in the TiO_2 absorption range, the photoresponse of tissues impregnated with TiO_2 hydrosol-S2 was greater than that presented by tissues impregnated with TiO_2 hydrosol-S1, and gravimetric measurements showed that the amounts of TiO_2 in the coated fabrics were very similar, Table 1. Therefore, the differences in the optical absorption was attributed to larger particle sizes of TiO_2-S2 (Fig. 2), which results in lower scattering coefficients and higher K-M function values when they have the same absorption coefficient (Jiménez Reinosa, Leret, Álvarez-Docio, del Campo & Fernández, 2016; Tan et al., 2013).

The DRS curves (Fig. 3 and Figure S3) also showed cutting wavelengths for samples TiO_2-S1, TiO_2-S2, TiO_2-S1-cotton, TiO_2-S2-cotton, TiO_2-S1-NWF and TiO_2-S2- NWF equal to 380, 377, 368, 357, 401 and 402 nm, respectively. This different values indicated that the absorption of TiO_2 varied when this was impregnated in the fabrics due to the interaction between the particles and the substrate (Kisch & Weiß, 2002; Tan et al., 2013; Zhang et al., 2020). Moreover, all DRS curves of the impregnated fabrics showed a slight tail wavelength larger than 400 nm, which was attributed to the presence of defects or surface impurities

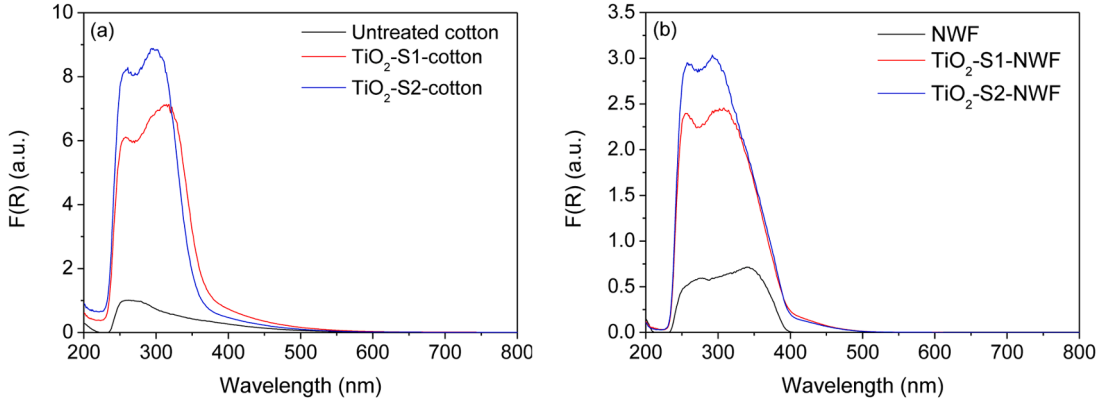

Fig. 3. Diffuse reflectance spectra UV–visible curves (a) for untreated cotton, TiO_2-S1-cotton and TiO_2-S2-cotton and (b) for non-woven fabric, TiO_2-S1-NWF and TiO_2-S2-NWF.

over the less crystallized TiO_2 nanoparticles (Jiang, Long, Wu & Cai, 2011).

Additionally, the band gap energies of TiO_2-S1 (3.16 eV) and TiO_2-S2 (3.17 eV), Figure S3, were close to the value assigned for the indirect band gap of the anatase phase (3.20 eV) (Lin et al., 2006; López & Gómez, 2012). It is worth mentioning that the indoor light used to evaluate de virucidal effect of coated fabrics presented a very small amount of irradiation at wavelength $\lambda < 400$ nm (Figure S1), and could lead to poor photoactivation of the TiO_2 particles (Rodríguez-González et al., 2020).

The FTIR spectra obtained for both synthesized TiO_2 samples (TiO_2-S1 and TiO_2-S2), Figure S4, were very similar and presented the same absorption bands at 3384, 2920, 1625, 1527, 1427, 790, 663 and 484 cm^{-1}. The broad band centered on 3384 cm^{-1} and another band at 1630 cm^{-1} was assigned to the vibrations of the O−H stretch and OH bend, respectively, demonstrating the presence of water physically attached to the surface of the samples (Z. Wang et al., 2020). Additionally, characteristic peaks of the O–Ti–O and Ti−O−Ti bonds occurred around 790, 663 and 484 cm^{-1}. The bands observed at 1427 and 1527 cm^{-1} were related to −COO− antisymmetric and symmetric stretching, respectively (Z. Wang et al., 2020). These bands were assigned to the carboxyl groups present on the surface of the TiO_2 samples provenient from the acetic acid used in the synthesis of hydrosol (Liao, Lien & Lin, 2001). The small peaks centered on 2930 and 2850 cm^{-1} were attributed to the asymmetric stretching vibrations of aliphatic C−H, confirming the existence of organic species adsorbed on the surface of TiO_2 particles, such as residues of acetic acid originating from the synthesis method. These results indicated that the surface of TiO_2 obtained from hydrosol presented functional important groups such as –OH and –COOH, which facilitated the retention of the particles within the fibers of the fabrics. Although the TiO_2 particles showed traces of adsorbed residual organic species, the virucidal effect caused by these was below the detection limit both under indoor illumination and dark conditions as shown in Section 3.2.

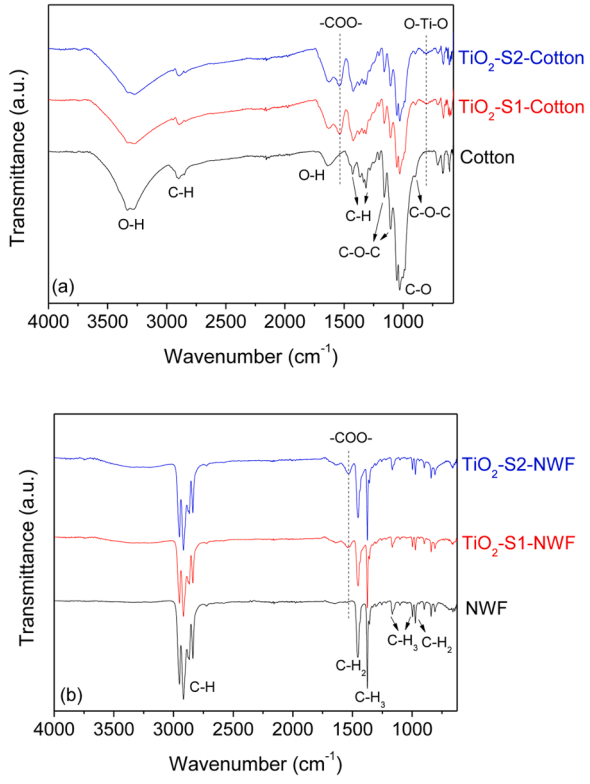

Fig. 4. FTIR-ATR absorbance spectra of coated and uncoated cotton (a) and non-woven (b) fabrics.

Chemical surface modification of the cotton and NWF fabrics by coating with TiO_2 hydrosol S1 and S2 was studied by FTIR-ATR analysis, Fig. 4. Pristine cotton, Fig. 4(a), presented a spectra characteristic of cellulose (Ahmad et al., 2019; Nam et al., 2016; Tudu, Sinhamahapatra & Kumar, 2020): 3600–3000 cm^{-1} (O–H stretching vibration of H-bonded hydroxyl groups); 1641 cm^{-1} (O–H stretching vibration of adsorbed water); 2901 cm^{-1} (C–H asymmetric stretching of alkyl chain); 1426 cm^{-1} (C–H bending); 1311 cm^{-1} (C–H wagging); 1160 and 1101 cm^{-1} (asymmetric bridge C–O–C); 1026 cm^{-1} (C–O stretch) and 896 cm^{-1} (asymmetric stretching of C1–O–C4 of cellulose) (Ahmad et al., 2019). The spectra of TiO_2-coated cotton presented the same bands of uncoated cotton and more two new peaks at 1535 cm^{-1} and 791 cm^{-1}. These peaks related to the −COO− symmetric stretching and O–Ti–O bonds (see the TiO_2 FTIR spectra in Figure S4) indicated the attachment of TiO_2 on the cotton fabric surface.

As expected, the uncoated NWF fabric, Fig. 4b, showed the characteristic peaks of polypropylene (Cabello-Alvarado et al., 2019; Cerkez, Worley, Broughton & Huang, 2013; Nam et al., 2016). In the range from 3000 to 2800 cm^{-1}, the bands corresponded to the asymmetric and symmetric C−H stretching vibration of methylene (CH_2) and methyl (CH_3) groups (Cabello-Alvarado et al., 2019). The peaks corresponding to bending of CH_2 and CH_3 bonds were localized at 1453 cm^{-1} and 1376 cm^{-1}, respectively (Cabello-Alvarado et al., 2019). Both coated NWF fabrics (Fig. 4(b)) presented a new band at 1530 cm^{-1} related to −COO− symmetric stretching, an important functional group that can indicate the presence of TiO_2 on the fabric surface.

The surface area analysis of TiO_2-S1 and TiO_2-S2 particles (Figure S5) generated type IV adsorption/desorption isotherms with an H_2 hysteresis loop, typical of mesoporous adsorbents according to the IUPAC classification (Burwell, 1977). The average pore size calculated by the BJH method (Table 2) was 43.87 and 37.29 nm for TiO_2-S1 and TiO_2-S2, respectively, which confirms the mesoporous characteristic of the TiO_2 samples synthetized (Burwell, 1977). The specific surface areas of the TiO_2-S1 and TiO_2-S2 particles were 293.1 and 342.4 $m^2\ g^{-1}$, respectively (Table 2). The surface area increased and the pore size decreased due to the reduction of the particle size particles (Table 2) which was expected when a smaller amount of Ti precursor was used in the synthesis (Nyamukamba et al., 2018). When the hydrosols were deposited on the fabrics, the specific surface area of the coated materials (Figure S6) increased by one (cotton) to two (NWF) order of magnitude due to the presence of the high surface area TiO_2 particles (Table 2).

The hydrophilicity of the coated surface is important and affects the contact between TiO_2 particles and viruses. Since TiO_2 typically has a hemispherical-like morphology, the virulence effect by mechanical damage due to contact relates to the size of the particles that are able to cover or permeate the cell wall (Rodríguez-González et al., 2020). This characteristic was investigated since the structures of human adenovirus type 5 (HAdV-5) and the murine coronavirus MHV-3 strain (MHV-3) were significantly different. All coated fabrics were highly hydrophobic with contact angle values of 123.66°, 122.32°, 114.55° and 129.39° for TiO_2-S1-cotton, TiO_2-S2-cotton, TiO_2-S1-NWF and TiO_2-S2-NWF, respectively (Fig. 5) under indoor illumination. The contact angle is quite similar to that measured under dark conditions (Figure S7), being 123.78°, 121.87°, 122.91° and 119.330°, for TiO_2-S1-cotton, TiO_2--S2-cotton, TiO_2-S1-NWF and TiO_2-S2-NWF, respectively. Fig. 5 and S7 show no changes in the water drops shapes when the samples are under dark or indoor light conditions. These results indicate that the irradiated indoor light surfaces do not generate sufficient electron-hole pairs to increase the hydrophilicity of the coated fabrics, and the supplementary hydroxyl groups and oxygen vacancies were not produced under indoor light.

3.2. Virucidal activity

Cell integrity and cytotoxic effects were evaluated, as described in the experimental section. The samples showed no cytotoxic effect in the

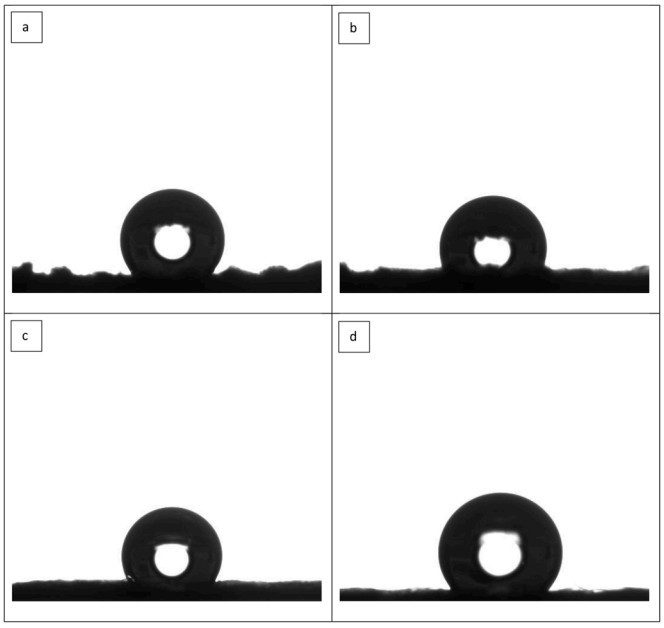

Fig. 5. Image of water droplets from tissue samples (a) TiO_2-S1-cotton, (b) TiO_2-S2-cotton, (c) TiO_2-S1-NWF and (d) TiO_2-S2-NWF.

assays, keeping more than 50% as viable cells. The virucidal activity of the treated fabrics (Table 3) under indoor light show higher inactivation of MHV-3 in comparison with HAdV-5, while the uncoated fabrics showed no activity. One reason for these results can be attributed to the hydrophobic interactions that are involved in the adsorption of the viruses on the surface of the coated fabrics, causing distortion of the viral shape (Li et al., 2016; Moon et al., 2020) and consequently inducing inactivation. This surface effect was especially important for the samples coated with TiO_2-S2 since significant virucidal activity was also observed under dark conditions (Table 3). In fact, the HAdV-5 particles have an icosahedral capsid (~90 nm in diameter) formed by proteins (Alonso-Padilla et al., 2016), while MHV-3 are enveloped, spherical or pleiomorphic viruses, with typical sizes ranging from 80 to 120 nm (Belouzard et al., 2012). Differently than HAdV-5, the MHV-3 virus has an envelope that contains at least three viral proteins, and the genome is packaged into a helical nucleocapsid surrounded by a host-derived lipid bilayer. Therefore, it could be expected that the MHV-3 virus interacts at a greater range with hydrophobic surfaces than HAdV-5 causing a higher rate of effective viral deactivation.

The virucidal activity was more significant on the fabrics coated with TiO_2-S2-NWF rather than TiO_2-S1-NWF under dark conditions, and was similar under indoor illumination. Considering that both coatings presented similar light absorption properties and band gaps, we attributed this to the concerted effect of the higher surface area of TiO_2-S2-NWF than TiO_2-S1-NWF (Table 2). Thus, the viruses may be inactivated by the rupture of its membrane caused by the distortion of the viral form when these were adsorbed on the surface of the photocatalyst (Kumar & Devi, 2011; Mohan et al., 2021). Moreover, a catalyst with a high specific surface area allows a greater number of active sites, where viruses can be adsorbed, distorted and attacked by photogenerated ROS (Hajkova, Spatenka, Horsky, Horska & Kolouch, 2007; Ishiguro et al., 2011; Koizumi & Taya, 2002; Nakano et al., 2013), that developed an important effect under indoor illumination.

Nakano et al. (2013) have reported that the virucidal activity of photocatalytic inactivation also depends on the viral envelop, since non-enveloped viruses are more resistant to inactivation than enveloped viruses (Beekes, Mielke, Pauli, Baier & Kurth, 2004; Jafry, Liga, Li & Barron, 2011). This could explain why MHV-3 virus was inactivated with a higher efficiency in comparison to HAdV-5. It is supposed that the photocatalytic action of TiO_2 would promote peroxidation of phospholipid components of the enveloped membrane, causing damage membrane and further virus inactivation (Beekes et al., 2004; Rutala & Weber, 2008). The results pointed to a reduction in the viral genomes of HAdV-2 and MHV-3 in the fabrics (Fig. 6), indicating that there was indeed a reduction in viral replication, which could be mediated by genome degradation and/or protein degradation of the viral envelope.

In untreated tissues, there was the detection of viral genomes within cells with viral entry and replication (Fig. 6). Although the attack to the viral genome by TiO_2 - photocatalytic reactions has been proposed as the mechanism capable of inactivating pathogenic viruses (Tong et al., 2021), inactivation could also be caused by damage of the outer viral proteins structure (Hajkova et al., 2007; Ishiguro et al., 2011; Koizumi & Taya, 2002) by reactive oxygen species produced during TiO_2 photocatalysis. Beside this, the photocatalytic activity also depends on the virus adsorption on the solid surface (Jafry et al., 2011), that would increase with the surface area of the photocatalyst.

SEM images of uncoated and coated cotton and non-woven fabrics are presented in Figs. 7 and 8. In the images of pristine cellulose-based cotton (Fig. 7) the characteristic fibers of this material are evident (Ibrahim et al., 2017; P. Wang et al., 2018). A smooth film of TiO_2 particles was observed on the cotton fabrics with TiO_2-S1 and TiO_2-S2 although the film presented several clusters (some highlighted by red circles) and cracks (some highlighted by red arrows). The presence of TiO_2 promoted an increase in the surface area of the coated cotton fabric in the order of 10 times (10 $m^2\ g^{-1}$ for TiO_2-S1-cotton and 9 $m^2\ g^{-1}$ for TiO_2-S2-cotton) compared to untreated cotton (<< 1 $m^2\ g^{-1}$), Table 2.

Similarly, an evenly distributed TiO_2 film was observed over the NWF fibers (Fig. 8). The coating of polypropylene NWF with TiO_2 particles caused a more significant increase in the surface area of these fabric samples (51 $m^2\ g^{-1}$ for TiO_2-S1-NWF; 110 $m^2\ g^{-1}$ for TiO_2-S2-NWF and 0.9 $m^2\ g^{-1}$ for untreated NWF), Table 2. The images show that TiO_2 particles were more homogeneously distributed over the fibers of NWF than over the cotton fibers, with less or almost no formation of agglomerates. This effect may have contributed to the greater increase in the surface area of the NWF coated with TiO_2 in comparison to the coated cotton fabric.

Table 3
Virus reduction in textile surfaces treated with TiO_2 (S1 and S2) under indoor light and under dark conditions.

Samples	HAdV-5 PFU/cm^2	MHV-3 PFU/cm^2	Indoor light		Dark conditions	
			HAdV-5 reduction (%)	MHV-3 reduction (%)	HAdV-5 reduction (%)	MHV-3 reduction (%)
TiO_2-S1-Cotton	$1.5 \times 10^5 \pm 1.1 \times 10^1$	$1.5 \times 10^4 \pm 1.1 \times 10^1$	NR	97.69 ± 0.16	*	*
TiO_2-S2-Cotton	$1.4 \times 10^5 \pm 2.3 \times 10^1$	$2.8 \times 10^4 \pm 2.3 \times 10^1$	NR	95.69 ± 0.34	*	*
TiO_2-S1-NWF	$1.1 \times 10^4 \pm 1.2 \times 10^1$	$1.1 \times 10^2 \pm 1.2 \times 10^1$	90.83 ± 1.00	99.98 ± 0.19	NR	NR
TiO_2-S2-NWF	$1.1 \times 10^4 \pm 1.2 \times 10^1$	$3.2 \times 10^2 \pm 1.2 \times 10^1$	90.83 ± 1.00	99.94 ± 0.19	90.00 ± 1.00	90.00 ± 1.00
Untreated/ Control Cotton	$1.5 \times 10^5 \pm 2.0 \times 10^1$	$6.5 \times 10^5 \pm 2.0 \times 10^1$	NR	NR	*	*
Untreated/ Control NWF	$1.2 \times 10^5 \pm 1.3 \times 10^1$	$6.2 \times 10^5 \pm 1.3 \times 10^1$	NR	NR	*	*

NR: No reduction.
* Not measured.

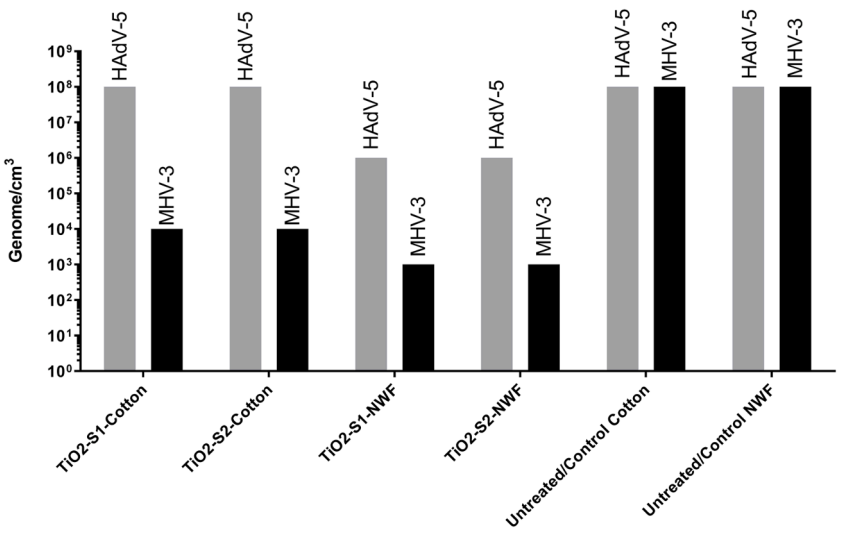

Fig. 6. Genome quantification of HAdV-5 and MHV-3 post in vitro cell infection in textile surfaces treated with TiO_2 (S1 and S2) under indoor light and conditions.

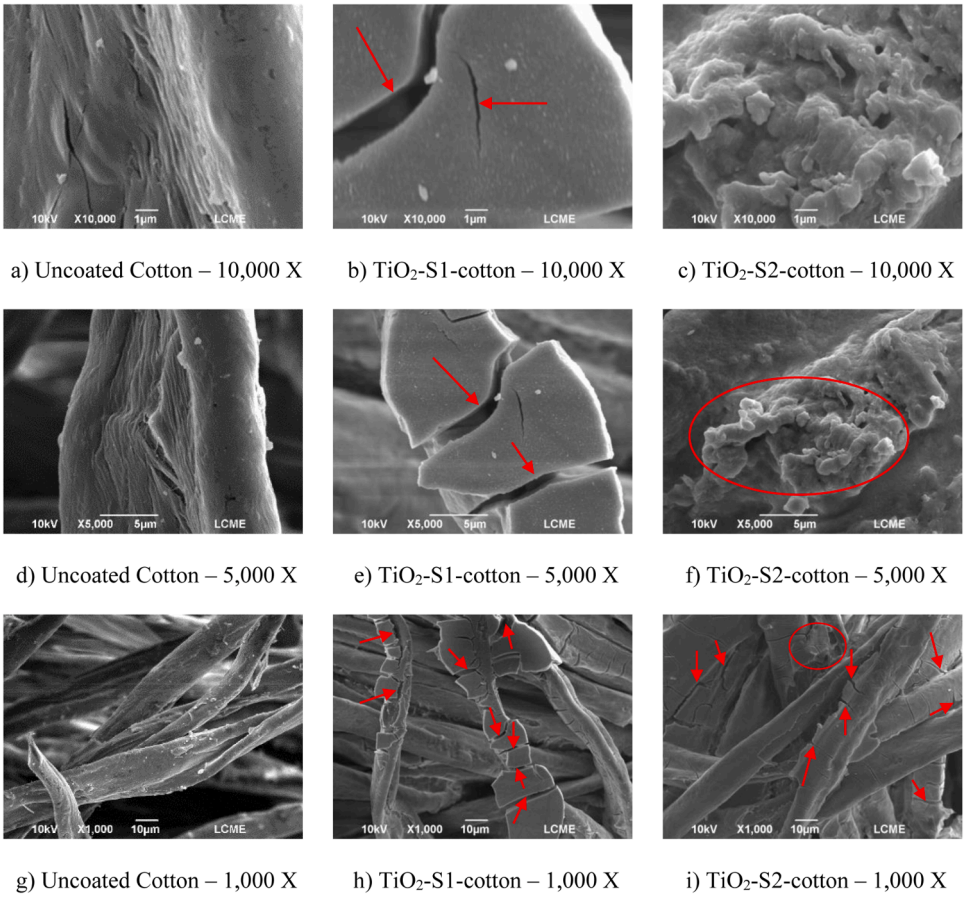

Fig. 7. SEM analysis for uncoated and coated cotton fabric samples in different magnifications: a–c) Magnification 10,000 X; d–f) Magnification 5000 X; and g–i) Magnification 1000 X (Uncoated cotton, TiO_2-S1-cotton and TiO_2-S2-cotton, respectively).

Although the amount of TiO_2-S1 and TiO_2-S2 particles deposited on the fabrics were similar (Table 1), the virucidal activities on NWF fabric were higher than those measured on cotton, due to more uniform distribution of TiO_2 particles on the NWF fabric solid surface, as shown in Figs. 7 and 8. These results implied that viral particles of HAdV-5 and MHV-3 could be efficiently inactivated using TiO_2 under indoor light.

Although several polysaccharides such as chitosan (Modak, Jha & Kumar, 2021), an acid polysaccharide from Laminaria japonica (Yue et al., 2017), and polysaccharides from algae (Harden, Falshaw, Carnachan, Kern & Prichard, 2009) have shown virucidal activity, cellulose-based fabric alone did not present virucidal activity (Table 3). However, cellulose can strongly attach TiO_2 particles through the formation of intermolecular hydrogen bonding between the hydroxyl group of cellulose and the hydroxyl group in the TiO_2 surface (Chai,

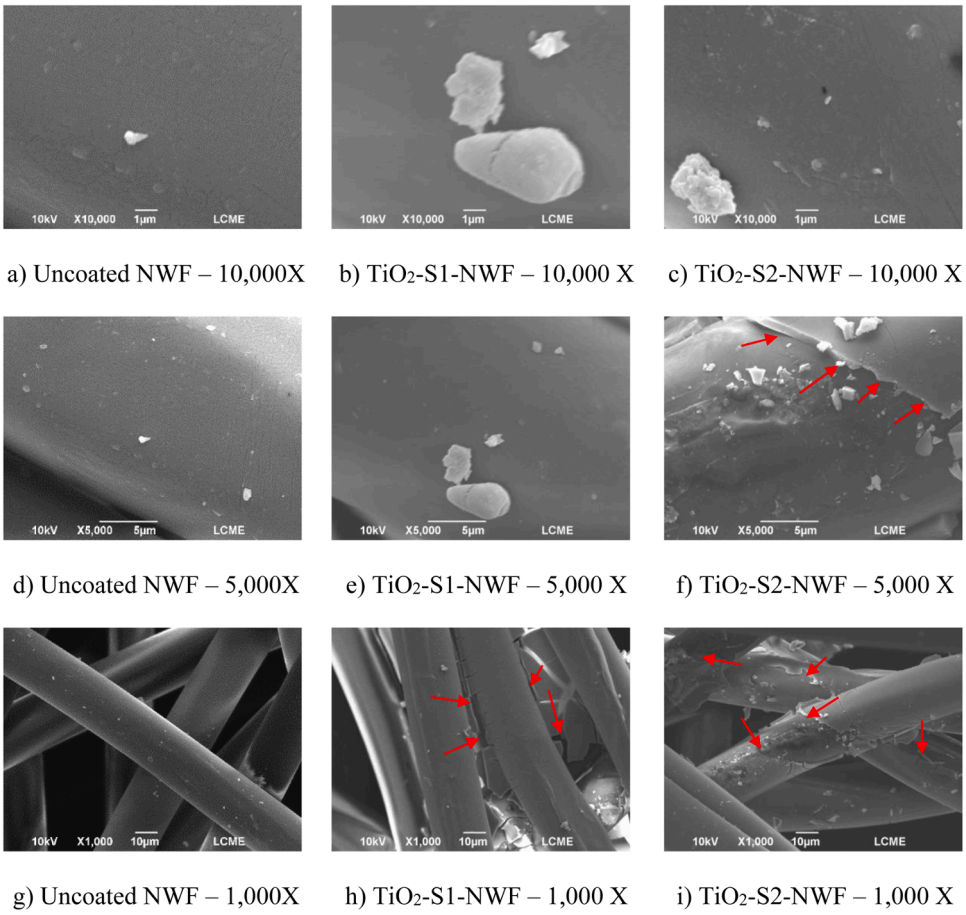

Fig. 8. SEM analysis for uncoated and coated polypropylene non-woven fabric samples in different magnifications: a–c) Magnification 10,000 X; d–f) Magnification 5000 X; and g–i) Magnification 1000 X (Uncoated NWF, TiO_2-S1-NWF and TiO_2-S2-NWF, respectively).

Pang, Lim & Chong, 2021; Zong et al., 2021) even those produced using a hydrolysis-precipitation method (Zong et al., 2021), and the materials exhibited antibacterial properties.

As largely known, TiO_2 particles inactivate influenza virus (Nakano et al., 2012), human coronavirus (Tong et al., 2021), bovine coronavirus (Yoshizawa et al., 2020), human norovirus, murine norovirus (Park et al., 2016), SARS coronavirus (Han et al., 2004), and bacteriophage (Syngouna et al., 2017), among others. These effects may involve reactive oxygen species that can damage viral surface proteins, what in turn may impair of even abolish the adsorption of the viruses to host cells as well as to damage the viral genome, preventing the replication process. So, the attachment of TiO_2 particles on cellulose fibers could be useful to produce virucidal fabrics. Hospital supplies made with non-woven fabric are usually disposable. However, hospital cotton items are usually washed and reused. In the latter case, the cotton fabric covered with TiO_2 generally presents a low level of wash resistance due to the poor adhesion between the TiO_2 particles and the fibers (Dastjerdi, Montazer & Shahsavan, 2009; Wang et al., 2018).

The virucidal activity was also performed after one cycle washing of TiO_2-coated fabrics. The TiO_2-treated cotton and TiO_2-treated NWF were submerged in pure water under magnetic stirring for 1 h. After this, the samples were dried and submitted to virucidal tests, resulting in similar virus inactivation.

The results in this study collectively reveal the photocatalytic inactivation mechanism of HAdV-5 and MHV-3 by TiO_2 under standard indoor light irradiation. The high surface area of TiO_2 and the hydrophobicity of coated fabrics could contribute to the antiviral properties. Proteins oxidation by ROS formed under indoor light irradiation also contributes to virus inactivation, although the interaction of MHV-3 and HAdV-5 on TiO_2-S2 coated fabrics would be enough for some virus inactivation. The hydrophobic characteristic of the treated fabrics and the high surface area of TiO_2 particles favor interaction with the virus, mainly MHV-3.

Although the sol-gel based TiO_2 particles of large area have been applied for various biological applications (Amanulla et al., 2019; Chegeni, Pour & Dizaji, 2019; Dinesh, Suresh Yadav, Kannadasan & Rasool, 2017), a deeper study about cytotoxic effect should be performed to guarantee their potential impact on environmental health and safety (Rashid et al., 2021).

4. Conclusions

High surface area and mesoporous TiO_2 particles were successfully prepared using the sol-gel method. The study found that non-woven fabric, coated with high surface area TiO_2 particles, exhibited remarkable virucidal effects on both the human adenovirus type 5 (HAdV-5) and the murine coronavirus MHV-3 strain under indoor light and room temperature. Inactivation of the MHV-3 virus (a lipid bilayer enveloped virus) occurred more efficiently than that of the HAdV-5 virus. The virucidal effect increased as the surface area of the particles was increased and the average particle size was decreased. These observations indicate that hydrophobic interactions with the TiO_2 particles and/or adsorption on the TiO_2 immobilized particles are important for developing effective virucidal fabrics. The TiO_2 hydrosol can, thus, be regarded as an effective photocatalytic agent for producing virucidal fabrics, with higher efficiency when applied on non-woven fabric than on cotton. Photocatalytic TiO_2-based nanomaterials are nowadays restricted to research laboratories, but the results obtained in this work

are likely to represent a significant contribution to their industrial and operational application.

Associated content

Supporting information

Spectrum of LED lamp used in this work (Figure S1); ; SEM-FEG and TEM images (Figure S2); diffuse reflectance spectroscopy analysis of powdered TiO_2 (Figure S3); FTIR absorbance spectra of powdered TiO_2 (Figure S4); adsorption-desorption isotherms of powdered TiO_2 (Figure S5) and tissue samples (Figure S6); images of water droplets from tissue samples under dark conditions (Figure S7).

Author contributions

Darliane Souza: Validation; Investigation; Writing - Original Draft
Suélen M. Amorim: Methodology; Validation; Formal analysis; Investigation; Writing - Original Draft
Rafael D. Cadamuro: Formal analysis; Investigation; Visualization
Gislaine Fongaro: Validation; Formal analysis; Visualization
Rosely A. Peralta: Methodology; Formal analysis; Writing - Review & Editing.
Rosane M. Peralta: Formal analysis; Writing – Review & Editing.
Gianluca Li Puma: Formal analysis; Writing – Review and Editing.
Regina de F P M Moreira: Conceptualization; Methodology; Formal analysis; Resources; Writing - Review & Editing; Supervision; Project administration

Declaration of Competing Interest

The authors declare that they have no known competing financial interests or personal relationships that could have appeared to influence the work reported in this paper.

Acknowledgement

This research was supported by the Coordination for the Improvement of Higher Education Personnel (CAPES-PRINT Project number 88887.310560/2018–00 and CAPES Finance code 001), National Council for Technological and Scientific Development (CNPq/Brazil), and by other partners at UFSC (LINDEN, LCME and the Central of Analysis at EQA/UFSC).

Supplementary materials

Supplementary material associated with this article can be found, in the online version, at doi:10.1016/j.carpta.2021.100182.

References

Ahmad, I., Kan, C., & Yao, Z. (2019). Photoactive cotton fabric for UV protection and self-cleaning. *RSC Advances, 9*(32), 18106–18114. https://doi.org/10.1039/C9RA02023C

Alonso-Padilla, J., Papp, T., Kaján, G. L., Benkő, M., Havenga, M., Lemckert, A., et al. (2016). Development of novel adenoviral vectors to overcome challenges observed with HAdV-5–based constructs. *Molecular Therapy, 24*(1), 6–16. https://doi.org/10.1038/mt.2015.194

Amanulla, A. M., & Sundaram, R. (2019). Green synthesis of TiO_2 nanoparticles using orange peel extract for antibacterial, cytotoxicity and humidity sensor applications. *Materials Today, 8*, 323–331. https://doi.org/10.1016/j.matpr.2019.02.118

Beekes, M., Mielke, M., Pauli, G., Baier, M., & Kurth, R. (2004). Aspects of risk assessment and risk management of nosocomial transmission of classical and variant Creutzfeldt-Jakob disease with special attention to German regulations. *In Prions, 11*, 117–135. https://doi.org/10.1159/000077053 (pp.

Belouzard, S., Millet, J. K., Licitra, B. N., & Whittaker, G. R. (2012). Mechanisms of coronavirus cell entry mediated by the viral spike protein. *Viruses, 4*(6), 1011–1033. https://doi.org/10.3390/v4061011

Besselsen, D. G., Wagner, A. M., & Loganbill, J. K. (2003). Detection of lymphocytic choriomeningitis virus by use of fluorogenic nuclease reverse transcriptase-polymerase chain reaction analysis. *Comparative Medicine, 53*, 65–69.

Burwell, R. L. (1977). Manual of symbols and terminology for physicochemical quantities and units—Appendix II heterogeneous catalysis. *Advances in Catalysis, 26*, 351–392. https://doi.org/10.1016/S0360-0564(08)60074-7

Cabello-Alvarado, C., Reyes-Rodríguez, P., Andrade-Guel, M., Cadenas-Pliego, G., Pérez-Alvarez, M., Cruz-Delgado, V. J., et al. (2019). Melt-mixed thermoplastic nanocomposite containing carbon nanotubes and titanium dioxide for flame retardancy applications. *Polymers, 11*(7), 18. https://doi.org/10.3390/polym11071204

Cerkez, I., Worley, S. D., Broughton, R. M., & Huang, T. S. (2013). Antimicrobial surface coatings for polypropylene nonwoven fabrics. *Reactive and Functional Polymers, 73*(11), 1412–1419. https://doi.org/10.1016/j.reactfunctpolym.2013.07.016

Chai, Y. D, Pang, Y. L, Lim, S, & Chong, W. C (2021). Sonocatalytic degradation of Congo Red using biomass-based cellulose/TiO2 composite. *Materials Today, 42*(1), 50–55. https://doi.org/10.1016/j.matpr.2020.09.246

Chegeni, M., Pour, S. K., & Dizaji, B. F. (2019). Synthesis and characterization of novel antibacterial sol-gel derived TiO_2/Zn_2TiO_4/Ag nanocomposite as an active agent in sunscreens. *Ceramics International, 45*(8), 24413–24418. https://doi.org/10.1016/j.ceramint.2019.08.163

Dastjerdi, R., Montazer, M., & & hahsavan, S. (2009). A new method to stabilize nanoparticles on textile surfaces. *Colloids and Surfaces A: Physicochemical and Engineering Aspects, 345*, 202–210. https://doi.org/10.1016/j.colsurfa.2009.05.007. http://doi.org/.

De Pasquale, I., Lo Porto, C., Dell'Edera, M., Petronella, F., Agostiano, A., Curri, M. L., et al. (2020). Photocatalytic TiO_2-based nanostructured materials for microbial inactivation. *Catalysts, 10*(12), 47. https://doi.org/10.3390/catal10121382

Dicastillo, C. L., de, Correa, M. G., Martínez, F. B., Streitt, C., & Galotto, M. J. (2020). Antimicrobial effect of titanium dioxide nanoparticles. *IntechOpen, 1*, 1–18. https://doi.org/10.5772/intechopen.90891

Dinesh, P., Suresh Yadav, C., Kannadasan, S., & Rasool, M. (2017). Cytotoxicity and immunomodulatory effects of sol-gel combustion based titanium dioxide (TiO_2) particles of large surface area on RAW 264.7 macrophages. *Toxicology in Vitro, 43*, 92–103. https://doi.org/10.1016/j.tiv.2017.06.006

Erdem, A., Metzler, D., Cha, D., & Huang, C. P. (2015). Inhibition of bacteria by photocatalytic nano-TiO_2 particles in the absence of light. *International Journal of Environmental Science and Technology, 12*(9), 2987–2996. https://doi.org/10.1007/s13762-014-0729-2

Gerrity, D., Ryu, H., Crittenden, J., & Abbaszadegan, M. (2008). Photocatalytic inactivation of viruses using titanium dioxide nanoparticles and low-pressure UV light. *Journal of Environmental Science and Health, Part A,, 43*(11), 1261–1270. https://doi.org/10.1080/10934520802177813

Grabherr, S., Ludewig, B., & Pikor, N. B. (2021). Insights into coronavirus immunity taught by the murine coronavirus. *European Journal of Immunology, 51*(5), 1062–1070. https://doi.org/10.1002/eji.202048984

Hajkova, P., Spatenka, P., Horsky, J., Horska, I., & Kolouch, A. (2007). Photocatalytic effect of TiO_2 films on viruses and bacteria. *Plasma Processes and Polymers, 4*(S1), S397–S401. https://doi.org/10.1002/ppap.200731007

Hamouda, T., Ibrahim, H. M., Kafafy, H. H., Mashaly, H. M., Mohamed, N. H., & Aly, N. M. (2021). Preparation of cellulose-based wipes treated with antimicrobial and antiviral silver nanoparticles as novel effective high-performance coronavirus fighter. *International Journal of Biological Macromolecules, 181*, 990–1002. https://doi.org/10.1016/j.ijbiomac.2021.04.071

Han, W., Zhang, B., Cao, W., Yang, D., Taira, I., Okamoto, Y., et al. (2004). The inactivation effect of photocatalytic titanium apatite filter on SARS virus. *Progress in Biochemistry and Biophysics, 31*, 982–985.

Harden, E. A., Falshaw, R., Carnachan, S. M., Kern, E. R., & Prichard, M. N. (2009). Virucidal activity of polysaccharide extracts from four algal species against herpes simplex virus. *Antiviral Research, 83*(3), 282–289. https://doi.org/10.1016/j.antiviral.2009.06.007

Hernroth, B. E., Conden-Hanson, A. C., Rehnstan-Holm, A. S., Girones, R., & Allard, A. K. (2002). Environmental factors influencing human viral pathogens and their potencial indicator organisms in the blue mussel. Mytilus edulis: The first Scadinavian report *Applied and Environmental Microbiology, 68*(9), 4523–4533. https://doi.org/10.1128/AEM.68.9.4523-4533.2002.

Hosseini, M., Chin, A. W. H., Behzadinasab, S., Poon, L. L. M., & Ducker, W. A. (2021). Cupric oxide coating that rapidly reduces infection by SARS-CoV-2 via solids. *ACS Applied Materials & Interfaces, 13*(5), 5919–5928. https://doi.org/10.1021/acsami.0c19465

Ibrahim, N. A., Aly, A. A., Eid, B. M., & Fahmy, H. M. (2018a). Green approach for multifunctionalization of cellulose-containing fabrics. *Fibers and Polymers, 19*(11), 2298–2306. https://doi.org/10.1007/s12221-018-8602-4

Ibrahim, N. A., Eid, B. M., El-Aziz, E. A., Abou Elmaaty, T. M., & Ramadan, S. M. (2017). Multifunctional cellulose-containing fabrics using modified finishing formulations. *RSC Advances, 7*(53), 33219–33230. https://doi.org/10.1039/C7RA05403C

Ibrahim, N. A., Eid, B. M., Khalil, H. M., & Almetwally, A. A. (2018b). A new approach for durable multifunctional coating of PET fabric. *Applied Surface Science, 448*, 95–103. https://doi.org/10.1016/j.apsusc.2018.04.022

Ibrahim, N. A., Nada, A. A., Eid, B. M., Al-Moghazy, M., Hassabo, A. G., & Abou-Zeid, N. Y. (2018c). Nano-structured metal oxides: Synthesis, characterization and application for multifunctional cotton fabric. *Advances in Natural Sciences: Nanoscience and Nanotechnology, 9*(3), 11. https://doi.org/10.1088/2043-6254/aadc2c, 035014.

International Organization for Standardization. (2019). ISO 18184:2019 textiles — Determination of antiviral activity of textile products (pp. 1–41).

Ishiguro, H., Nakano, R., Yao, Y., Kajioka, J., Fujishima, A., Sunada, K., et al. (2011). Photocatalytic inactivation of bacteriophages by TiO2-coated glass plates under low-intensity, long-wavelength UV irradiation. *Photochemical & Photobiological Sciences, 10*(11), 1825–1829. https://doi.org/10.1039/c1pp05192j

Jafry, H. R., Liga, M. V., Li, Q., & Barron, A. R. (2011). Simple route to enhanced photocatalytic activity of P25 titanium dioxide nanoparticles by silica addition. *Environmental Science & Technology, 45*(4), 1563–1568. https://doi.org/10.1021/es102749e

Jiang, J., Long, M., Wu, D., & Cai, W. (2011). Alkoxyl-derived visible light activity of TiO_2 synthesized at low temperature. *Journal of Molecular Catalysis A: Chemical, 335* (1–2), 97–104. https://doi.org/10.1016/j.molcata.2010.11.019

Jiménez Reinosa, J., Leret, P., Álvarez-Docio, C. M., del Campo, A., & Fernández, J. F. (2016). Enhancement of UV absorption behavior in ZnO–TiO2 composites. *Boletín de La Sociedad Española de Cerámica y Vidrio, 55*(2), 55–62. https://doi.org/10.1016/j.bsecv.2016.01.004

Khaiboullina, S., Uppal, T., Dhabarde, N., Subramanian, V. R., & Verma, S. (2020). vitro inactivation of human coronavirus by titania nanoparticle coatings and UVC radiation: Throwing light on SARS-CoV-2. *bioRxiv, 13*(1), 19. https://doi.org/10.1101/2020.08.25.265223

Khezerlou, A., Alizadeh-Sani, M., Azizi-Lalabadi, M., & Ehsani, A. (2018). Nanoparticles and their antimicrobial properties against pathogens including bacteria, fungi, parasites and viruses. *Microbial Pathogenesis, 123*, 505–526. https://doi.org/10.1016/j.micpath.2018.08.008

Kisch, H., & Weiß, H. (2002). Tuning photoelectrochemical and photocatalytic properties through electronic semiconductor–support interaction. *Advanced Functional Materials, 12*(8), 483–488, 10.1002/1616-3028(20020805)12:8<483::AID-ADFM483>3.0.CO;2-K.

Kleebusch, E., Patzig, C., Krause, M., Hu, Y., Höche, T., & Rüssel, C. (2018). The effect of TiO_2 on nucleation and crystallization of a Li_2O-Al_2O_3-SiO_2 glass investigated by XANES and STEM. *Scientific Reports, 8*(1), 8. https://doi.org/10.1038/s41598-018-21227-x

Koizumi, Y., & Taya, M. (2002). Kinetic evaluation of biocidal activity of titanium dioxide against phage MS2 considering interaction between the phage and photocatalyst particles. *Biochemical Engineering Journal, 12*(2), 107–116. https://doi.org/10.1016/S1369-703X(02)00046-3

Kumar, S. G., & Devi, L. G. (2011). Review on modified TiO_2 photocatalysis under UV/visible light: Selected results and related mechanisms on interfacial charge carrier transfer dynamics. *The Journal of Physical Chemistry A, 115*(46), 13211–13241. https://doi.org/10.1021/jp204364a

Li, Y., Zhang, C., Shuai, D., Naraginti, S., Wang, D., & Zhang, W. (2016). Visible-light-driven photocatalytic inactivation of MS2 by metal-free g-C3N4: Virucidal performance and mechanism. *Water Research, 106*, 249–258. https://doi.org/10.1016/j.watres.2016.10.009

Liao, L.-. F., Lien, C.-. F., & Lin, J.-. L. (2001). FTIR study of adsorption and photoreactions of acetic acid on TiO_2. *Physical Chemistry Chemical Physics, 3*(17), 3831–3837. https://doi.org/10.1039/b103419g

Lin, H., Huang, C., Li, W., Ni, C., Shah, S., & Tseng, Y. (2006). Size dependency of nanocrystalline TiO_2 on its optical property and photocatalytic reactivity exemplified by 2-chlorophenol. *Applied Catalysis B: Environmental, 68*(1–2), 1–11. https://doi.org/10.1016/j.apcatb.2006.07.018

Liu, L., John, B., Yeung, K. L., & Si, G. (2007). Non-UV based germicidal activity of metal-doped TiO_2 coating on solid surfaces. *Journal of Environmental Sciences, 19*(6), 745–750. https://doi.org/10.1016/S1001-0742(07)60124-7

Liu, Y., Huang, J., Feng, X., & Li, H. (2021). Thermal-sprayed photocatalytic coatings for biocidal applications: A review. *Journal of Thermal Spray Technology, 30*(1–2), 1–24. https://doi.org/10.1007/s11666-020-01118-2

López, R., & Gómez, R. (2012). Band-gap energy estimation from diffuse reflectance measurements on sol-gel and commercial TiO_2: A comparative study. *Journal of Sol-Gel Science and Technology, 61*(1), 1–7. https://doi.org/10.1007/s10971-011-2582-9

Mazurkova, N. A., Spitsyna, Y. E., Shikina, N. V., Ismagilov, Z. R., Zagrebel'nyi, S. N., & Ryabchikova, E. I. (2010). Interaction of titanium dioxide nanoparticles with influenza virus. *Nanotechnologies in Russia, 5*(5–6), 417–420. https://doi.org/10.1134/S1995078010050174

Metcalf, T. G., Melnick, J. L., & Estes, M. K. (1995). Environmental virology: From detection of virus in sewage and water by isolation to identification by molecular biology — A trip of over 50 years. *Annual Review of Microbiology, 49*, 461–487. https://doi.org/10.1146/annurev.mi.49.100195.002333

Modak, C., Jha, A. N., & Kumar, A. (2021). Chitosan derivatives: A suggestive evaluation for novel inhibitor discovery against wild type and variants of SARS-CoV-2 virus. *International Journal of Biological Macromolecules, 187*, 492–512. https://doi.org/10.1016/j.ijbiomac.2021.07.144

Mohan, S. V., Hemalatha, M., Kopperi, H., Ranjith, I., & Kumar, A. K. (2021). SARS-CoV-2 in environmental perspective: Occurrence, persistence, surveillance, inactivation and challenges. *Chemical Engineering Journal, 405*, 21. https://doi.org/10.1016/j.cej.2020.126893, 126893.

Moon, E. W., Lee, H.-. W., Rok, J. H., & Ha, J.-. H. (2020). Photocatalytic inactivation of viral particles of human norovirus by Cu-doped TiO_2 non-woven fabric under UVA-LED wavelengths. *Science of the Total Environment, 749*, 9. https://doi.org/10.1016/j.scitotenv.2020.141574, 141574.

Nakano, R., Hara, M., Ishiguro, H., Yao, Y., Ochiai, T., Nakata, K., et al. (2013). Broad spectrum microbicidal activity of photocatalysis by TiO_2. *Catalysts, 3*(1), 310–323. https://doi.org/10.3390/catal3010310

Nakano, R., Ishiguro, H., Yao, Y., Kajioka, J., Fujishima, A., Sunada, K., et al. (2012). Photocatalytic inactivation of influenza virus by titanium dioxide thin film. *Photochemical & Photobiological Sciences : Official Journal of the European Photochemistry Association and the European Society for Photobiology, 11*, 1293–1298. https://doi.org/10.1039/c2pp05414k

Nam, S., Slopek, R., Wolf, D., Warnock, M., Condon, B. D., Sawhney, P., et al. (2016). Comparison of biodegradation of low-weight hydroentangled raw cotton nonwoven fabric and that of commonly used disposable nonwoven fabrics in aerobic Captina silt loam soil. *Textile Research Journal, 86*(2), 155–166. https://doi.org/10.1177/0040517514551468

Nyamukamba, P., Okoh, O., Mungondori, H., Taziwa, R., & Zinya, S. (2018). Synthetic methods for titanium dioxide nanoparticles: A review. In titanium dioxide - material for a sustainable environment. 10.5772/intechopen.75425.

Park, D., Shahbaz, H. M., Kim, S. H., Lee, M., Lee, W., Oh, J. W., et al. (2016). Inactivation efficiency and mechanism of UV-TiO_2 photocatalysis against murine norovirus using a solidified agar matrix. *International Journal of Food Microbiology, 238*, 256–264. https://doi.org/10.1016/j.ijfoodmicro.2016.09.025

Park, G. W., Cho, M., Cates, E. L., Lee, D., Oh, B.-. T., Vinjé, J., et al. (2014). Fluorinated TiO_2 as an ambient light-activated virucidal surface coating material for the control of human norovirus. *Journal of Photochemistry and Photobiology B: Biology, 140*, 315–320. https://doi.org/10.1016/j.jphotobiol.2014.08.009

Person, B. D., John, L., Rafie, K., Strebl, M., Fransmyr, L., Ballmann, M. Z., et al. (2021). Human species D Adenovirus hexon capsid protein mediates cell entry through a direct interaction with CD46. *Proceedings of the National Academy of Sciences of the United States of America, 118*(3), 8. https://doi.org/10.1073/pnas.2020732118. e2020732118.

Rabenau, H. F., Steinmann, J., Rapp, I., Schwebke, I., & Eggers, M. (2014). Evaluation of a virucidal quantitative carrier test for surface disinfectants. *PloS one, 9*(1), 10. https://doi.org/10.1371/journal.pone.0086128. E86128.

Rashid, M. M., Simoncic, B., & Tomsic, B. (2021). Recent advances in TiO_2-functionalized textile surfaces. *Surfaces and Interfaces, 22*, 33. https://doi.org/10.1016/j.surfin.2020.100890, 100890.

Rodríguez-González, V., Obregón, S., Patrón-Soberano, O. A., Terashima, C., & Fujishima, A. (2020). An approach to the photocatalytic mechanism in the TiO_2-nanomaterials microorganism interface for the control of infectious processes. *Applied Catalysis B: Environmental, 270*, 21. https://doi.org/10.1016/j.apcatb.2020.118853, 118853.

Rutala, W. A., & Weber, D. J. (2008). Healthcare infection control practices advisory committee (HICPAC). In guideline for disinfection and sterilization in healthcare facilities. *Centers for disease control and prevention (CDC)*.

Syngouna, V. I., & Chrysikopoulos, C. V. (2017). Inactivation of MS2 bacteriophage by titanium dioxide nanoparticles in the presence of quartz sand with and without ambient light. *Journal of Colloid and Interface Science, 497*, 117–125. https://doi.org/10.1016/j.jcis.2017.02.059

Tan, B., Gao, B., Guo, J., Guo, X., & Long, M. (2013). A comparison of TiO_2 coated self-cleaning cotton by the sols from peptizing and hydrothermal routes. *Surface and Coatings Technology, 232*, 10. https://doi.org/10.1016/j.surfcoat.2013.04.048

Tong, Y., Shi, G., Hu, G., Hu, X., Han, L., Xie, X., et al. (2021). Photo-catalyzed TiO_2 inactivates pathogenic viruses by attacking viral genome. *Chemical Engineering Journal, 414*, Article 128788. https://doi.org/10.1016/j.cej.2021.128788

Tudu, B. K., Sinhamahapatra, A., & Kumar, A. (2020). Surface modification of cotton fabric using TiO_2 nanoparticles for self-cleaning, oil–water separation, antistain, anti-water absorption, and antibacterial properties. *ACS Omega, 5*(14), 7850–7860. https://doi.org/10.1021/acsomega.9b04067

Uyguner Demirel, C. S., Birben, N. C., & Bekbolet, M. (2018). A comprehensive review on the use of second generation TiO_2 photocatalysts: Microorganism inactivation. *Chemosphere, 211*, 420–448. https://doi.org/10.1016/j.chemosphere.2018.07.121

Wang, P., Dong, Y., Li, B., Li, Z., & Bian, L. (2018). A sustainable and cost effective surface functionalization of cotton fabric using TiO_2 hydrosol produced in a pilot scale : Condition optimization, sunlight-driven photocatalytic activity and practical applications. *Industrial Crops & Products, 123*, 197–207. https://doi.org/10.1016/j.indcrop.2018.06.067

Wang, Z., Yu, Q., Gauvin, F., Feng, P., Qianping, R., & Brouwers, H. J. H. (2020). Nanodispersed TiO_2 hydrosol modified Portland cement paste: The underlying role of hydration on self-cleaning mechanisms. *Cement and Concrete Research, 136*, 14. https://doi.org/10.1016/j.cemconres.2020.106156, 106156.

Yoshizawa, N., Ishihara, R., Omiya, D., Ishitsuka, M., Hirano, S., & Suzuki, T. (2020). Application of a photocatalyst as an inactivator of bovine coronavirus. *Viruses, 12*, 10. https://doi.org/10.3390/v12121372

Yue, Y., Li, Z., Li, P., Song, N., Li, B., Lin, W., et al. (2017). Antiviral activity of a polysaccharide from Laminaria Japonica against Enterovirus 71. *Biomedicine & Pharmacotherapy, 96*, 256–262. https://doi.org/10.1016/j.biopha.2017.09.117

Zan, L., Fa, W., Peng, T., & Gong, Z. (2007). Photocatalysis effect of nanometer TiO_2 and TiO_2-coated ceramic plate on Hepatitis B virus. *Journal of Photochemistry and Photobiology B: Biology, 86*(2), 165–169. https://doi.org/10.1016/j.jphotobiol.2006.09.002

Zhang, H., Tang, Q., Li, Q., Song, Q., Wu, H., & Mao, N. (2020). Enhanced photocatalytic properties of PET filaments coated with Ag-N Co-doped TiO_2 nanoparticles sensitized with disperse blue dyes. *Nanomaterials, 10*(5), 24. https://doi.org/10.3390/nano10050987

Zong, E., Wang, C., Yang, J., Zhu, H., Jiang, S., Liu, X., et al. (2021). Preparation of TiO_2/cellulose nanocomposites as antibacterial bio-adsorbents for effective phosphate removal from aqueous medium. *International Journal of Biological Macromolecules, 182*, 434. https://doi.org/10.1016/j.ijbiomac.2021.04.007